Heliyon 9 (2023) e22605

Contents lists available at ScienceDirect

Heliyon

journal homepage: www.cell.com/heliyon

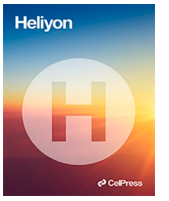

Repurposing fluphenazine as an autophagy modulator for treating liver cancer

Chang Su [a,b,1], Cai-yan Cheng [a,c,1], Zheng Rong [a,1], Jing-cheng Yang [a], Zhi-mei Li [c], Jing-yue Yao [a], An Liu [a], Le Yang [a,**], Ming-gao Zhao [a,c,*]

[a] Precision Pharmacy & Drug Development Center, Department of Pharmacy, Tangdu Hospital, Air Force Military Medical University, Xi'an, China
[b] Shaanxi Provincial Corps, Chinese People's Armed Police Force, Xi'an, China
[c] Institute of Medical Research, Northwestern Polytechnical University, Xi'an, China

ARTICLE INFO

Keywords:
Hepatocellular carcinoma
Connectivity map
Fluphenazine
Autophagy
Drug repurposing
Chronic pain

ABSTRACT

Hepatocellular carcinoma (HCC) is a common malignant tumor of the digestive system with a low early diagnosis rate. Owing to the side effects, tolerance, and patient contraindications of existing therapies, effective drug treatments for HCC remain a major clinical challenge. However, using approved or investigational drugs not initially intended for cancer therapy is a promising strategy for resolving this problem because their safety have been tested in clinic. Therefore, this study evaluated differentially expressed genes between liver cancer and normal tissues in a cohort of patients with HCC from The Cancer Genome Atlas and applied them to query a connectivity map to identify candidate anti-HCC drugs. As a result, fluphenazine was identified as a candidate for anti-HCC therapy *in vitro* and *in vivo*. Fluphenazine suppressed HCC cell proliferation and migration and induced cell cycle arrest and apoptosis, possibly owing to disrupted lysosomal function, blocking autophagy flux. Additionally, *in vivo* studies demonstrated that fluphenazine suppresses HCC subcutaneous xenografts growth without causing severe side effects. Strikingly, fluphenazine could be used as an analgesic to alleviate oxaliplatin-induced pain as well as pain related anxiety-like behavior. Therefore, fluphenazine could be a novel liver cancer treatment candidate.

1. Introduction

Hepatocellular carcinoma (HCC) is a major malignant tumor of the digestive system, ranking third in cancer-related mortality and sixth in the incidence of new cases (905,677 new cases in 2020) worldwide, according to the World Health Organization's 2020 report [1]. However, the 5-year survival rate of patients with HCC could increase to more than 70 % if the disease is diagnosed and surgically treated in the early stage [2]. Unfortunately, most HCC patients, who are diagnosed as fast progression as in the advanced stage, are not suitable for surgery when diagnosed; therefore, they require drug treatments. Systemic therapies, such as tyrosine kinase inhibitors (TKIs) and immune checkpoint inhibitors (ICIs), have been approved for locally unresectable HCC, and their curative effects have

* Corresponding author. Precision Pharmacy & Drug Development Center, Department of Pharmacy, Tangdu Hospital, Air Force Military Medical University, Xi'an, China.
** Corresponding author.
E-mail addresses: yanglefmmu@163.com (L. Yang), minggao@fmmu.edu.cn (M.-g. Zhao).
[1] These authors share first authorship.

https://doi.org/10.1016/j.heliyon.2023.e22605
Received 17 May 2023; Received in revised form 8 November 2023; Accepted 15 November 2023
Available online 22 November 2023

improved compared to traditional treatment methods [3–5]. However, drug treatments for patients with HCC remain a major clinical problem owing to adverse reactions, poor tolerance, and contraindications to these therapies. Therefore, identifying new drugs for HCC treatment is a critical and urgent requirement.

Over the last decade, more than 100 anti-tumor drugs have been approved for clinical research in China [6], and the enthusiasm of researchers in this area has never been higher. However, few drugs have been approved for clinical use for many reasons, such as safety, efficacy, the research and development cycle, and cost. Therefore, researchers have begun to shift focus, investigating the anti-tumor activities of approved drugs since their safety has been verified over many years of clinical use [7,8]. There are already several examples of this, such as metformin (initially for type 2 diabetes) and disulfiram (initially for alcohol abuse), which have since been demonstrated to have anti-tumor activity [9,10].

In recent years, an increasing number of differentially expressed genes (DEGs) have been identified between tumor and normal tissues, and these gene expression profiles have been employed to identify potential anti-tumor drugs. Connectivity Map (CMap) is a resource that uses gene expression differences in human cells treated with different perturbagens (including small-molecule compounds, gene knockdown, and overexpression reagents) to establish a biological application database of the correlations between perturbagens, gene expression profiles, and diseases [11]. This method can identify new therapeutic indications for approved or investigational drugs outside the original scope. For example, using CMap, parbendazole was identified as a stimulator of bone differentiation through the induction of cytoskeletal changes and increased the expression and activity of bone morphogenetic protein 2 (i.e., BMP-2), indicating its suitability as a bone anabolic treatment [12]. **Chen *et al.*** also found that hyperforin promotes energy consumption and exerts anti-obesity effects by querying CMap using cold-induced gene expression data [13].

Therefore, this study investigated DEGs between liver cancer and normal tissues in a cohort of patients with HCC from The Cancer Genome Atlas (TCGA) and CMap to identify candidate anti-HCC drugs. This analysis identified fluphenazine, a commonly prescribed antipsychotic drug, as a candidate and assessed its anti-HCC activity *in vitro* and *in vivo*. We found that fluphenazine could inhibit liver cancer cell proliferation and migration. It also induced cell cycle arrest and apoptosis of HCC cells. In addition, we observed that fluphenazine could act as an autophagy modulator through affecting lysosome function. *In vivo* studies showed that fluphenazine obviously suppressed the growth of HCC subcutaneous xenografts and did not cause serious side effects. Importantly, we found that fluphenazine could effectively relieve oxaliplatin-induced chronic pain and pain-related anxiety-like behavior. Taken together, our findings support that fluphenazine might be a new candidate for treating liver cancer.

2. Materials and methods

2.1. Reagents

Fluphenazine dihydrochloride, SKF-86002, BH3Z1, CP55667, pilaralisib, penfluridol, suloctidil, isopropylphthalimide, flunisolide, NSC3852, bemegride, selamectin, 3-methyladenine (3-MA), chloroquine (CQ) and Oxaliplatin were purchased from Topscience (Shanghai, China). Cell cycle and apoptosis analysis kit and Annexin V-FITC apoptosis detection kit were purchased from Beyotime (Shanghai, China). Alanine aminotransferase assay kit (ALT) and aspartate aminotransferase assay kit (AST) were purchased from Nanjing Jiancheng Bioengineering Institute (Nanjing, China).

2.2. Cell culture

The human liver cancer cell lines HepG-2 and Huh-7 were obtained from Procell Life Science&Technology Co., Ltd. (Wuhan, China). The human HCC cell lines MHCC97-H and HCCLM-3 were obtained from Zhong Qiao Xin Zhou Biotechnology Co., Ltd. (Shanghai, China). The human normal liver cell line HL-7702 (L02) were obtained from Guan&Dao Biological Engineering Co., Ltd. (Shanghai, China). HepG-2 cell line was cultured in a specialized culture medium obtained from Procell Life Science&Technology Co., Ltd. (Cat. CM-0103; MEM (containing NEAA) + 10 % FBS + 1 % penicillin and streptomycin). Huh-7, MHCC97-H and HCCLM-3 cells were cultured in DMEM (Cytiva, Utah, USA) with 10 % FBS (Gibco, NY, USA) plus 1 % penicillin and streptomycin (Sangon, Shanghai, China). L02 cell line was cultured in RIPA 1640 medium (Cytiva, Utah, USA) with 10 % FBS plus 1 % penicillin and streptomycin. All of the cells were cultured under humidified condition with 5 % CO_2 at 37 °C. The authentication of these cell lines was performed via comparisons with the STR database.

2.3. Data Collection and DEGs analysis

RNA-sequencing expression (level 3) profiles and corresponding clinical information for HCC were obtained from the TCGA dataset (https://portal.gdc.com). Differentially expressed genes (DEGs) were analyzed for patients of TCGA-HCC cohort using the limma package in the R software (p value < 0.05, $|\log Fc| > 1$). The R software was employed to draw volcano plot (ggplot2 package) and clustering heatmap (pheatmap package, v1.0.12).

2.4. CMap query

To find compounds that possess potential anti-HCC activity, we generated gene signatures of the 150 top upregulated and downregulated DEGs in HCC patients and then entered into the “DOWN-regulated genes” and “UP-regulated genes” module of CMap. We identified multiple compounds and ranked according to the enrichment scores.

2.5. Cell viability assay and clonogenic assay

Cell viability assay was performed with a Cell Counting Kit-8 (EnoGene, Nanjing, China) according to the manufacturer's instructions. Briefly, cells were plated into 96-well plate at a concentration of 5×10^3 cells per well. After incubation for indicating time periods with different treatment, each well was added in 10 μl CCK-8 and 90 μl DMEM. The absorbance was measured at 450 nm after incubation for 40 min at 37 °C.

In clonogenic assay, HepG-2 cells were seeded into 6-well plates at a concentration of 700 cells per well and incubated overnight. After incubation with fluphenazine for 14 days, the cells were imaged using live cell imaging system (BIOTEK Cytation 1) to observe the size of clonies. Then, the cells were visualized by crystal violet (Beyotime, Shanghai, China) staining and clone numbers in each group were counted.

2.6. Migration assay

Transwell assay was conducted as previous described [14]. Briefly, 1×10^5 of MHCC97-H or HCCLM-3 cells in FBS-free medium were seeded in the upper transwell chamber (Corning, New York, USA) with indicated concentration of fluphenazine, and 600 μL DMEM with 20 % FBS containing equal concentration of fluphenazine was added in the lower chamber. After incubation for 24 h at 37 °C, cells on the bottom surface of the chamber were fixed using 4 % paraformaldehyde (Biosharp, Beijing, China) for 15 min and stained with 0.1 % crystal violet for 20 min, while the top surface of the chamber was wiped by a cotton swab to remove cells. The number of migrated cells were imaged and counted.

Wound-healing scratch assay was conducted as described previously [15]. Briefly, MHCC97-H cells were seeded in 6-well plates and incubated to 80 % confluency, then the cells were scratched by a 10 μL pipette followed with treatment of 5 μM or 10 μM fluphenazine in DMEM with 1 % FBS. The scratch wound was photographed at 0 h, 12 h, 24 h and 36 h after treatment and the migration distance was measured.

2.7. Cell cycle and apoptosis analysis

After treatment with fluphenazine for 48 h, the cells were fixed with 1 mL ice cold 70 % ethanol for 24 h and washed with ice cold PBS once. Then the cells were stained with 500 μL PI working buffer (500 μL staining buffer, 25 μL PI, 10 μL RNase A) for 30 min and cell cycle distribution was analyzed by FCM with NovoCyte (ACEA Biosciences Inc., San Diego, USA).

As for apoptosis analysis, the cells were harvested after treatment with fluphenazine for 48 h and suspended in 195 μL binding buffer followed by staining with 5 μL Annexin-V-FITC and 10 μL PI. The apoptotic cell rates were measured by FCM with NovoCyte.

2.8. Immunofluorescence

Cells were plated on round coverslip (Biosharp, Hefei, China) and fixed with 4 % paraformaldehyde for 30 min after treatment with fluphenazine for 48 h. The cells were cultured with enhanced immunostaining permeabilization solution (Beyotime, Shanghai, China) followed by blocking with 3 % goat serum for 1 h at room temperature. Then the cells were incubated with LC3B antibody (Novus, NBP2-46892, 1:100) overnight at 4 °C, and washed with PBS for 5 min three times. Finally, the cells were cultured with FITC-conjugated goat anti-rabbit IgG (Zhuangzhi bio, Xi'an, China) at room temperature for 1 h followed by staining with DAPI and imaged using a Nikon C2 plus confocal microscope.

2.9. LysoTracker staining

The cells were cultured with DMEM containing 100 nM LysoTracker Red DND-99 (MedChemExpress, USA) for 30 min at 37 °C after treatment with fluphenazine for 48 h. Then, the cells were fixed with 4 % paraformaldehyde for 30 min and stained with Hoechst 33342 solution (Solarbio, Beijing, China) for 20 min followed by imaging using a live cell imaging system (BIOTEK Cytation 1).

2.10. Western blotting analysis

Western blotting analysis was conducted as described previously [15]. Briefly, the cells were lysed in RIPA lysis buffer (Beyotime, Shanghai, China) with phosphatase inhibitor (Sangon Biotech, Shanghai, China) and proteinase inhibitor (Sangon Biotech, Shanghai, China). Proteins were separated using 10 % SDS-PAGE and transferred to PVDF membrane. After blocked with 5 % non-fat milk in TBST for 1 h at room temperature, membranes were incubated with primary antibody against cyclin D1 (rabbit; 55506s, Cell Signaling Technology, USA; 1:1000), cyclin E1 (rabbit; 20808s, Cell Signaling Technology, USA; 1:1000), p21 Waf2/Cip1 (rabbit; 2947s, Cell Signaling Technology, USA; 1:1000), p27 Kip1 (mouse; 3698s, Cell Signaling Technology, USA; 1:1000), CDK 2 (rabbit; 2546s, Cell Signaling Technology, USA; 1:1000), CDK 4 (rabbit; 12790s, Cell Signaling Technology, USA; 1:1000), Phospho-Akt (Ser473, rabbit; 4060s, Cell Signaling Technology, USA; 1:2000), Akt (pan, mouse; 2920s, Cell Signaling Technology, USA; 1:1000), Bcl-2 (rabbit; 3498s, Cell Signaling Technology, USA; 1:1000), Bax (rabbit; 14796s, Cell Signaling Technology, USA; 1:1000), Caspase-3 (rabbit; 14220s, Cell Signaling Technology, USA; 1:1000), Cleaved Caspase-3 (rabbit; 9664s, Cell Signaling Technology, USA; 1:1000), γ-H2AX (rabbit; ab81299, Abcam, UK; 1:5000), LC3B (rabbit; NBP2-46892, Novus, USA; 1:500), Beclin-1 (rabbit; ab207612, Abcam, UK; 1:2000), SQSTM1/p62 (rabbit; ab109012, Abcam, UK; 1:10000), β-actin (mouse; A5316, Sigma, USA; 1:5000) and GAPDH (mouse;

MB001, Bioworld Technology, USA; 1:5000) at 4 °C overnight. After washed with TBST for three times, membranes were incubated with secondary antibody (Goat Anti-Rabbit IgG or Goat Anti-Mouse IgG, HRP Conjugated; Zhuangzhi bio, Xi'an, China; 1:5000) for 1 h. Signals were detected using ChemiSignal® Plus Analysis Kit (CLINX, Shanghai, China) with ChemiScope Capture system (CLINX, Shanghai, China).

2.11. Subcutaneous xenograft models

All animal experiments in this study were approved and performed in strict accordance with the regulations of the Animal Care and Use Committee of the Fourth Military Medical University (ethical approval code for BALB/c nude mice: 20220449; ethical approval code for C57BL/6 mice: 20230669). Female BALB/c nude mice (5–6 week old, 18–22 g; The Fourth Military Medical University, Xi'an, China) were housed in a specific pathogen free environment under a 12 h light/12 h dark cycle. Subcutaneous xenograft models were performed as described previously [15]. Briefly, 5×10^6 MHCC97-H cells were injected into left-flanks of BALB/c nude mice. After injection with cells for 7 days, the mice were grouped (n = 6) based on the tumor volume as measured according to the following equation: volume = length (mm) × width $(mm)^2/2$ and administrated with fluphenazine (4 mg/kg or 8 mg/kg) or vehicle (sterile water for injections) once every 2 days via intraperitoneal injection (i.p.). Tumor volumes and body weights of the mice were measured every 4 days.

2.12. Immunohistological analysis

On the other day of the last administration, tumor tissues of mice from different groups were collected and fixed with 4 % paraformaldehyde followed by embedding in paraffin. The expression of Ki-67 (rabbit; 34330s, Cell Signaling Technology, USA; 1:200) was detected using IHC analysis and imaged using Slideview VS200 (Olympus).

2.13. Toxicity evaluation

On the other day of the fifth administration, we tested the effect of fluphenazine treatment on motor ability of mice using rotating rod method as previously described [16]. The mice were trained on the rotarod twice 2 days before the test and the time to fall was recorded. After 17 days of administration, the serum was harvested to analyze AST and ALT levels. Then, the mice were sacrificed and the heart, liver, spleen, lung, kidney and brain were collected followed by fixing in 4 % paraformaldehyde for H&E staining.

2.14. Oxaliplatin-induced chronic pain model and fluphenazine administration

Female C57BL/6 mice (5–6 week old, 20–25 g; The Fourth Military Medical University, Xi'an, China) were housed in a temperature-controlled environment under a 12 h light/dark cycle. Mice were randomly allocated to control or different experimental groups (n = 5). We established an oxaliplatin-induced chronic pain model as described previously [17]. Briefly, oxaliplatin or vehicle (0.5 % DMSO and sterile water for injections) was injected (i.p.) at 5.6 mg/kg once per day for five consecutive days. From the second day of modeling, fluphenazine or vehicle (sterile water for injections) was injected (i.p.) at 4 mg/kg once every 2 days for four times.

2.15. Paw withdrawal mechanical threshold test and thermal latency test

Mechanical hypersensitivity was evaluated by paw withdrawal threshold testing using a set of von Frey monofilaments (SA502, Jiangsu Cylon Biotechnology Co., LTD) as described previously [18,19]. Briefly, mice were placed on an elevated mesh-bottomed platform, allowing them to acclimate to it at least 1 h before the test. The threshold is considered to be the minimum force (0.008, 0.02, 0.04, 0.07, 0.16, 0.4, 0.6, 1.0, 1.4 and 2.0 g) to induce a rapid withdrawal response to five of the repeated stimuli for 10 consecutive times.

Thermal hypersensitivity was quantified by claw withdrawal testing using a device (KW-LB, Nanjing Calvin Biotechnology Co., LTD) as described previously [20]. Briefly, the mice were placed on a temperature-controlled board kept to 30 °C and the lateral plantar surface of hindpaw was stimulated with a radiant heat source at 55 °C. The time elapsed from initiation of the stimulus until paw withdrawal was defined as paw withdrawal thermal latency. The test was conducted three times to obtain the averaged withdrawal latency.

2.16. Open field (OF) test and elevated plus-maze (EPM) test

All tests were performed during the dark phase, and the light intensity was controlled under the same conditions. The mice were acclimated to the experimental instrument for 3h before each test, and the experimental environment was kept quiet. Before the next mouse was tested, the instrument was wiped clean with 70 % ethanol to avoid the influence of smell on the mice.

OF test was conducted as described previously [21]. Briefly, the mice were placed in the center of the experimental instrument ($40 \times 40 \times 40$ cm^3; VanBi-OF, Shanghai FanBI Intelligent Technology Co., LTD) and allowed to freely explore for 15 min. The exploratory behaviors of the mice were recorded using a camera fixed above the chamber. The distance and time traveled of mice in the center area and the total distance moved were recorded and analyzed using a video-tracking system (VanBi Tracking Master V3.0, Shanghai FanBI Intelligent Technology Co., LTD).

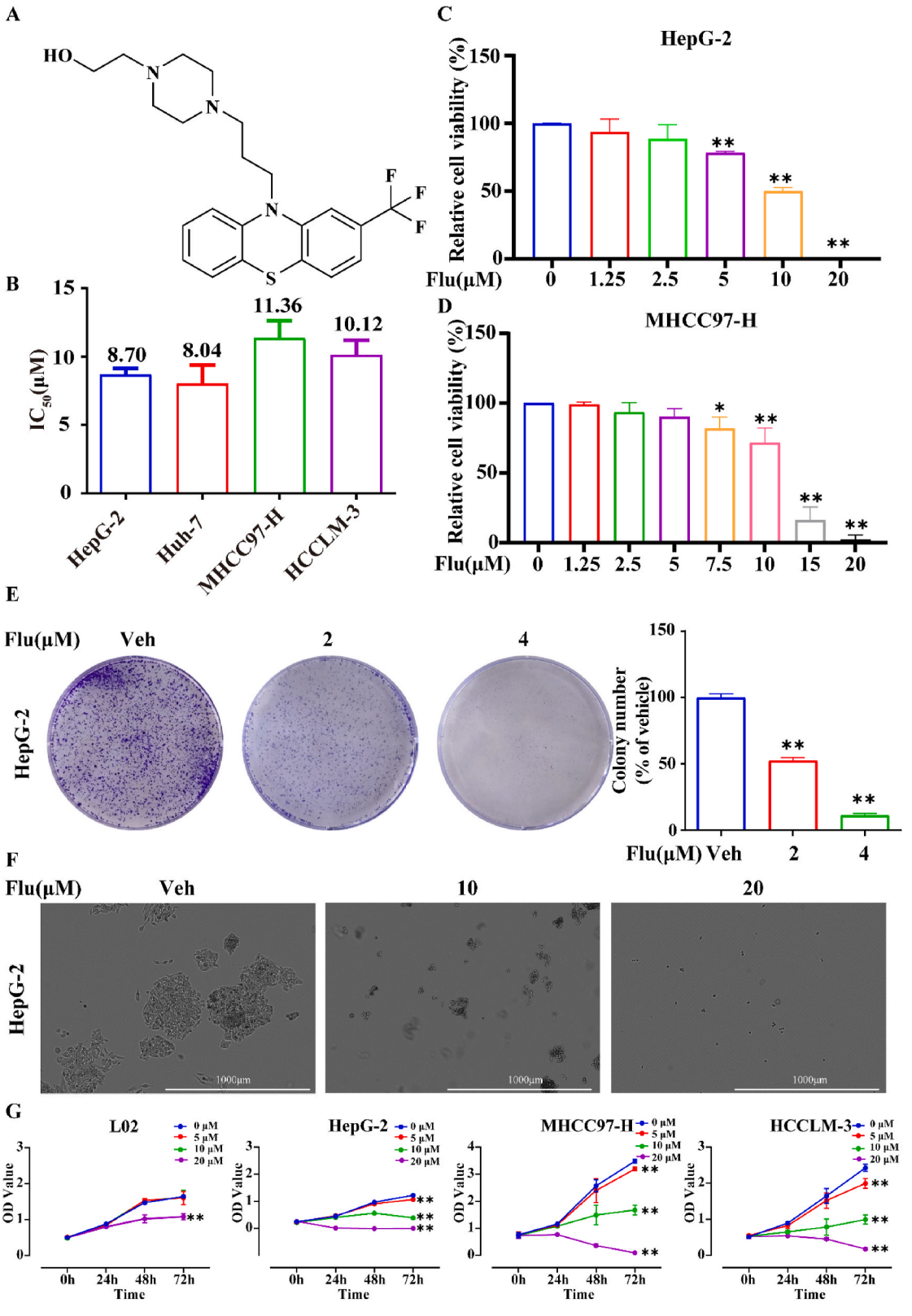

(caption on next page)

Fig. 1. Fluphenazine inhibits the growth and colony formation of HCC cells. (A) Chemical structure of fluphenazine. (B) IC_{50} values of fluphenazine against four HCC cell lines after 48 h of treatment (μM). (C) HepG-2 cells were treated with different concentrations of fluphenazine for 48 h, and the cell viabilities were measured using a cell count kit-8 (CCK-8) assay. (D) MHCC97-H cells were treated with different concentrations of fluphenazine for 48 h, and the cell viabilities were measured using an CCK-8 assay. (E, F) Inhibitory effects of fluphenazine on HepG-2 cells colony formation after 14 days of treatment. Images shown are representatives from three independent experiments. (G) The effects of different doses of fluphenazine treatment on the cell proliferation in normal liver cell line L02 and three HCC cell lines were conducted using CCK-8 assay. Data represent mean ± SD from at least three independent experiments (**$P < 0.01$).

EPM test was conducted as described previously [21] using an instrument (VanBi-OF, Shanghai FanBI Intelligent Technology Co., LTD) which consisted of two open arms ($25 \times 8 \times 0.5$ cm^3) and two closed arms ($25 \times 8 \times 12$ cm^3) that extended from a central platform (8×8 cm^2). For each test, each mouse was placed in the central area facing the open arm and subsequently allowed to explore freely for 5 min while being filmed with a camera fixed above the maze. The time spent in and the number of entries into the open and closed arms were recorded and analyzed with a video-tracking system (VanBi Tracking Master V3.0, Shanghai FanBI Intelligent Technology Co., LTD).

2.17. Statistical analysis

Data were represented as the mean ± standard deviation (SD) and processed using the GraphPad Prism 9. Two-tailed Student's *t*-

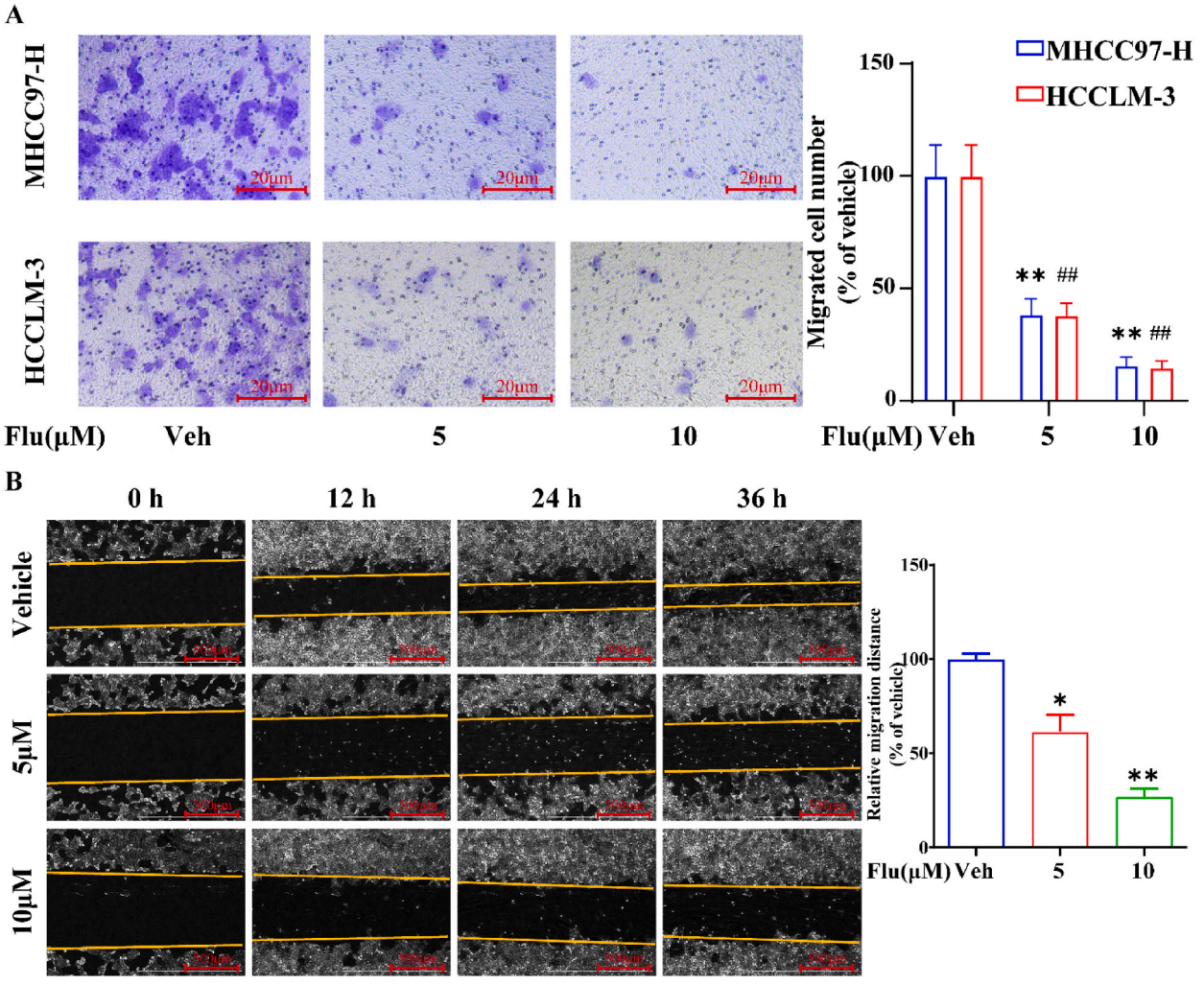

Fig. 2. Fluphenazine suppresses the migration of HCC cells. (A) Fluphenazine inhibited MHCC97-H and HCCLM-3 cells migration in transwell migration assay. Quantified values are shown on the right. (B) Fluphenazine inhibited MHCC97-H cells migration in wound-healing assay. Quantified values were shown on the right. Data represent mean ± SD from at least three independent experiments (MHCC97-H: vs vehicle * $P < 0.05$, **$P < 0.01$; HCCLM-3: vs vehicle $^{\#\#}P < 0.01$).

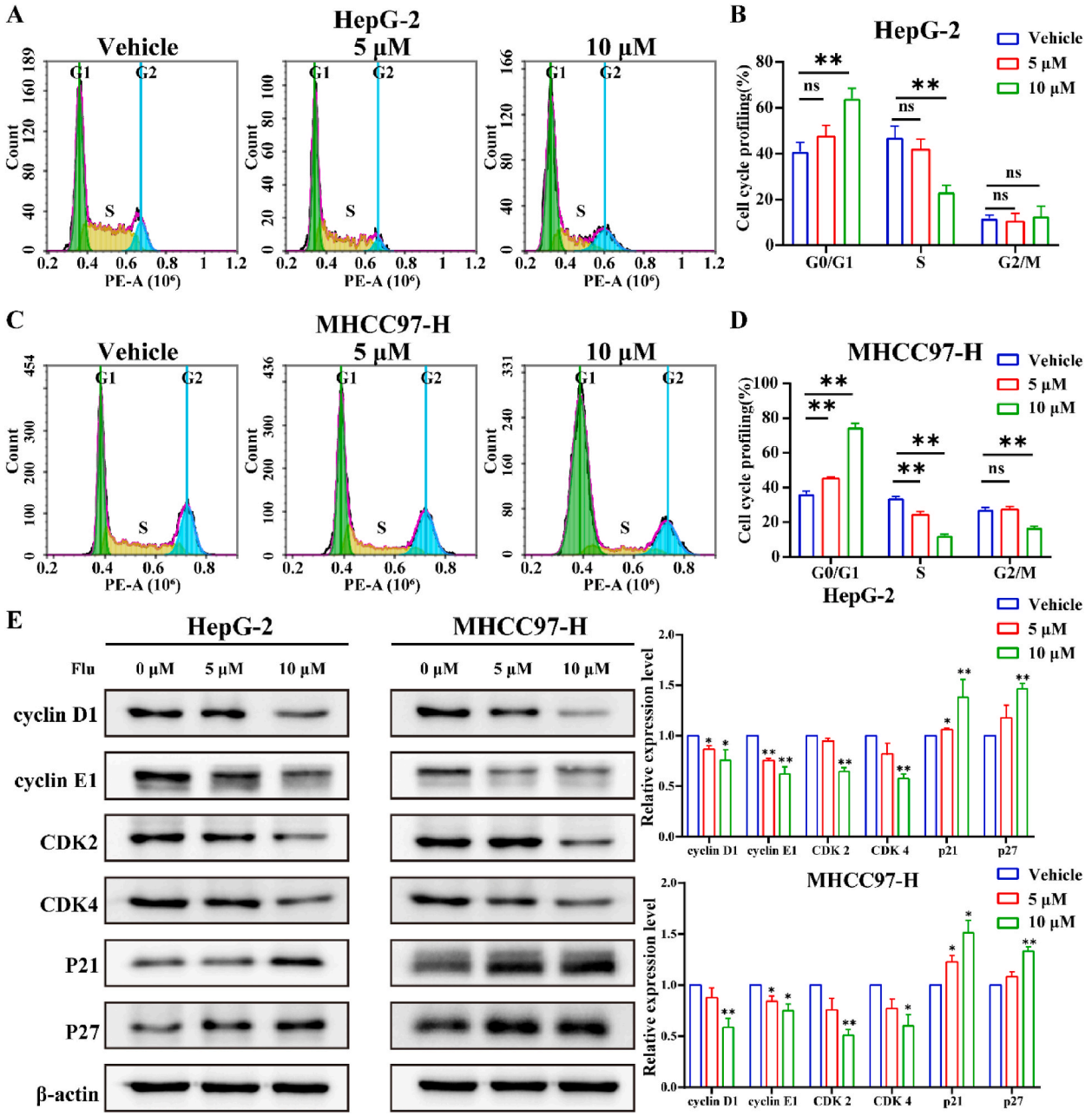

Fig. 3. Fluphenazine induced cell cycle G0/G1 phase arrest in HCC cells. (A) The cell cycle phase distributions of HepG-2 cells were analyzed using flux cytometry (FCM) after treatment with different concentrations of fluphenazine for 48 h. (B) Quantification of the percentage of cell cycle phase distributions after treatment with different concentrations of fluphenazine for 48 h in HepG-2 cells. (C) The cell cycle phase distributions of MHCC97-H cells were analyzed using FCM after treatment with different concentrations of fluphenazine for 48 h. (D) Quantification of the percentage of cell cycle phase distributions after treatment with different concentrations of fluphenazine for 48 h in MHCC97-H cells. (E) The expression of proteins involved in G0/G1 phase regulation was evaluated using Western blotting analysis in HepG-2 and MHCC97-H cells after treatment of fluphenazine for 48 h. Quantified values were shown on the right. Data represent mean ± SD from at least three independent experiments (*$P < 0.05$, **$P < 0.01$).

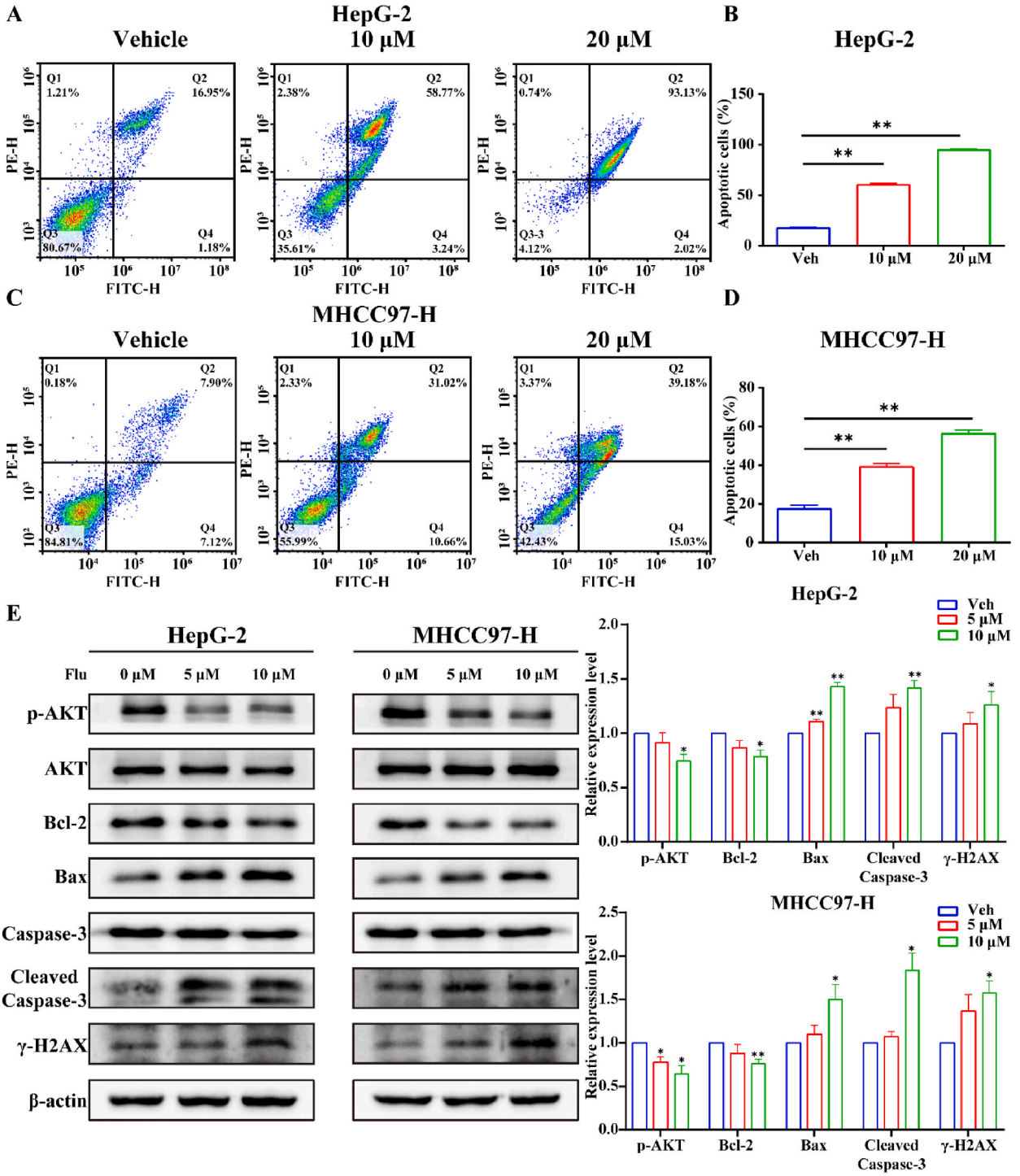

Fig. 4. Fluphenazine caused apoptosis in HCC cells. (A) The apoptosis analysis of HepG-2 cells was performed using FCM after treatment with different concentrations of fluphenazine for 48 h. (B) Quantification of the percentage of apoptotic cells after treatment with different concentrations of fluphenazine for 48 h in HepG-2 cells. (C) The apoptosis analysis of MHCC97-H cells was performed using FCM after treatment with different concentrations of fluphenazine for 48 h. (D) Quantification of the percentage of apoptotic cells after treatment with different concentrations of fluphenazine for 48 h in MHCC97-H cells. (E) The expression of apoptosis related proteins was evaluated using Western blotting analysis in HepG-2 and MHCC97-H cells after treatment of fluphenazine for 48 h. Quantified values were shown on the right. Data represent mean ± SD from at least three independent experiments (*$P < 0.05$, **$P < 0.01$).

test and One-way analysis of variance (ANOVA) were used to analyze the data. A P-value < 0.05 was considered statistically significant.

3. Results

3.1. Fluphenazine inhibited liver cancer cells growth and migration in vitro

To generate an HCC-specific RNA expression profile, we screened DEGs between tumor and normal tissues from patients with HCC from TCGA, obtaining 2395 upregulated (oncogenes) and 463 downregulated (tumor suppressor genes) genes (Supplementary Figs. 1A and B, Supplementary Table 1). The top 150 upregulated and downregulated DEGs (Supplementary Table 2) were entered into the "DOWN-regulated genes" and "UP-regulated genes" CMap modules, respectively. Consequently, we identified several compounds as potential anti-HCC drugs; Supplementary Fig. 1C presents the 25 top-ranking compounds based on their enrichment scores.

Next, we selected 12 commercially available compounds to evaluate their anti-HCC activity in two liver cancer cell lines, HepG-2 and MHCC97-H (Supplementary Figs. 1D and E). Of these, we found that fluphenazine, a classic antipsychotic drug, inhibited HCC cell viability; thus, it was selected for further investigation (Fig. 1A). The effects of fluphenazine on HCC cell growth were analyzed using four liver cancer cell lines; fluphenazine inhibited HCC cell survival (half maximal inhibitory values within 12 μM; Fig. 1B) and suppressed cell viability in a concentration-dependent manner (Fig. 1C and D; Supplementary Figs. 2A and B). Fluphenazine also remarkably reduced the number and size of HepG-2 cells in the micromolar range, as reflected by the colony formation assay (Fig. 1E and F). Additional cell proliferation analyses in a normal liver cell line (L02) and HCC cell lines were conducted to assess the toxicity of fluphenazine *in vitro*. Compared to the HCC cell lines, L02 cell proliferation was unaffected until 72 h after 5 μM or 10 μM fluphenazine treatment (Fig. 1G).

Supplementary Figure 1. Fluphenazine is identified as potential anti-HCC drugs using Connectivity Map (CMap) query. (A) The volcano plot of differentially expressed genes (DEGs) between tumor and normal tissues from HCC patients in The Cancer Genome Atlas (TCGA) cohort. Red dots indicate upregulated genes; blue dots indicate downregulated genes; grey dots indicate not significant. $P < 0.05$, $|\log Fc| > 1$. (B) The heatmap of the most significantly DEGs. (C) The 25 top-ranking compounds based on the enrichment scores of CMap query. (D) Inhibitory effects of 12 compounds on the viabilities of HepG-2 cells after 24 h or 48 h treatment (10 μM). (E) Inhibitory effects of 12 compounds on the viabilities of MHCC97-H cells after 24 h or 48 h treatment (10 μM). Data represent mean ± standard deviation (SD) from at least three independent experiments ($^*P < 0.05$, $^{**}P < 0.01$).

Supplementary Figure 2. Fluphenazine inhibits the growth of HCC cells. (A) Huh-7 cells were treated with different concentrations of fluphenazine for 48 h, and the cell viabilities were measured using an CCK-8 assay. (B) HCCLM-3 cells were treated with different concentrations of fluphenazine for 48 h, and the cell viabilities were measured using an CCK-8 assay. Data represent mean ± SD from at least three independent experiments.

We further examined the effect of fluphenazine on the migratory ability of HCC cells. Fluphenazine significantly inhibited the migration of two highly metastatic liver cancer cell lines (MHCC97-H and HCCLM-3) through the Transwell barrier (Fig. 2A); the wound-healing assay produced similar results (Fig. 2B).

Taken together, these results indicated that fluphenazine remarkably inhibited the growth and migration of liver cancer cells *in vitro*.

3.2. Fluphenazine caused G0/G1 arrest in HCC cells

A previous study demonstrated that fluphenazine induces G0/G1 arrest in breast cancer cells [22]. Therefore, we explored the effects of fluphenazine on the cell cycle of HCC cells, finding dose-dependent G0/G1 arrest after a 48-h treatment. In HepG-2 cells, the proportion of G0/G1 phase cells was 40.94 % in the vehicle group and 47.39 % and 64.10 % after 5 μM and 10 μM fluphenazine treatment, respectively (Fig. 3A and B). Similar results were observed in MHCC97-H cells (Fig. 3C and D). The expression levels of critical proteins involved in G1/S phase regulation were also examined; fluphenazine dose-dependently inhibited cyclin D1, cyclin E1, cyclin-dependent kinase (CDK) 2, and CDK4 expression after 48 h of treatment (Fig. 3E). In addition, fluphenazine upregulated P21 and P27 expression, two pivotal G1/S cell cycle transition inhibitors. Thus, this data implies that G0/G1 phase arrest contributes to the anticancer effects of fluphenazine.

3.3. Fluphenazine induced apoptosis in HCC cells

Apoptosis may also inhibit HCC cell proliferation after fluphenazine treatment. Therefore, we examined whether fluphenazine treatment caused HCC cell apoptosis. The ratio of apoptotic HepG-2 cells was remarkably higher after fluphenazine treatment (vehicle: 18.25 %, 10 μM fluphenazine: 61.10 %; 20 μM fluphenazine: 95.48 %; flow cytometry [FCM] analysis; Fig. 4A and B). Similar results were observed in MHCC97-H cells (Fig. 4C and D).

Next, we evaluated the expression of apoptosis-related proteins in fluphenazine-treated HCC cells. Fluphenazine concentration-dependently decreased B-cell lymphoma 2 (Bcl-2; anti-apoptotic) and increased Bax (pro-apoptotic) protein, cleaved-Capase-3, and γ-H2AX (an apoptosis indicator) expression in HCC cells (Fig. 4E).

The PI3K-Akt pathway is also involved in cell apoptosis [23], and studies indicated that fluphenazine inhibits breast cancer cell growth and migration by regulating the PI3K-Akt pathway [22]. Therefore, we examined the effect of fluphenazine on phosphorylated Akt expression, finding that it significantly decreased the expression of phosphorylated Akt (Fig. 4E). Thus, fluphenazine induces apoptosis in HCC cells.

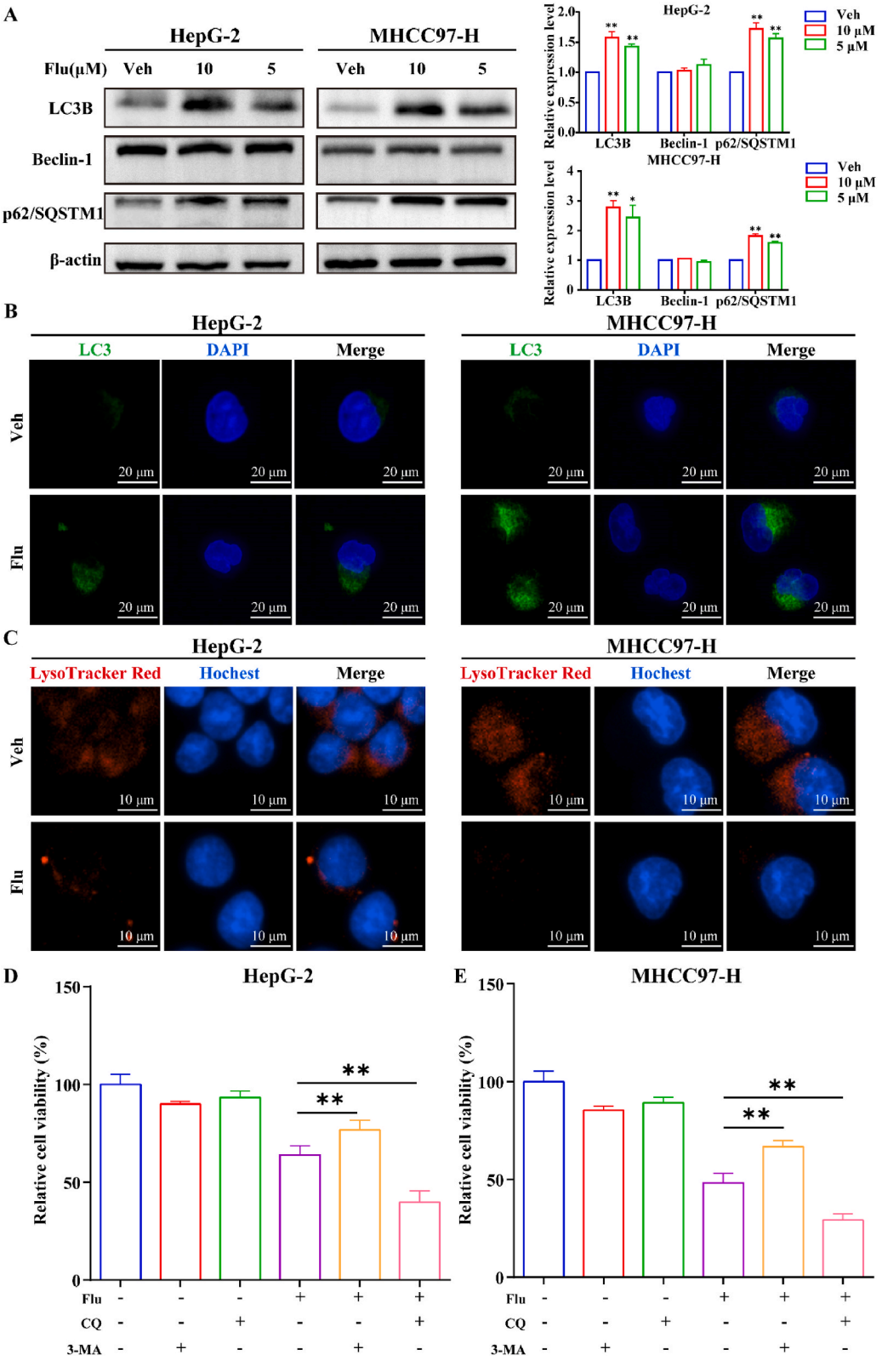

(caption on next page)

Fig. 5. Fluphenazine blocked autophagy flux of HCC cells. (A) The expression of autophagy related proteins was evaluated using Western blotting analysis in HepG-2 and MHCC97-H cells after treatment of fluphenazine for 48 h. Quantified values were shown on the right. (B) Confocal images of LC3B expression in HepG-2 and MHCC97-H cells treated with fluphenazine for 48 h. Nuclei were stained with DAPI. (C) Fluorescence images of LysoTracker Red in HepG-2 and MHCC97-H cells treated with fluphenazine for 48 h. Nuclei were stained with DAPI. (D) The cell viabilities of HepG-2 cells treated with 5 μM fluphenazine in the presence or absence of 1 mM 3-MA or 5 μM CQ for 48 h. (E) The cell viabilities of MHCC97-H cells treated with 10 μM fluphenazine in the presence or absence of 1 mM 3-MA or 5 μM CQ for 48 h. Data represent mean ± SD from at least three independent experiments (*$P < 0.05$, **$P < 0.01$).

3.4. Fluphenazine blocked autophagy flux in HCC cells by inhibiting lysosomal acidification

Next, we investigated the mechanism by which fluphenazine inhibits HCC cell growth. Autophagy changes often accompany cell proliferation inhibition and apoptosis, and previous studies have implicated fluphenazine as a potential autophagy modulator in cancer cells [24,25]. Therefore, we investigated the role of fluphenazine in autophagy regulation in HCC cells based on its effect on LC3B-II expression (an autophagy marker) in HCC cells. Type II LC3 protein expression was significantly higher in fluphenazine-treated HepG-2 and MHCC97-H cells than in the control group (Fig. 5A). This result was confirmed by immunofluorescence staining, which showed significantly increased LC3 expression and aggregation in fluphenazine-treated cells (Fig. 5B). However, fluphenazine did not affect Beclin-1 expression, a pivotal autophagosome formation protein, in HepG-2 and MHCC97-H cells, suggesting increased LC3 accumulation in HCC cells after fluphenazine treatment may be due to blocked autophagic flux rather than autophagy activation. Therefore, we measured p62/SQSTM1 expression, an autophagy substrate with a key role in autophagy, finding that p62/SQSTM1 protein expression increased in HepG-2 and MHCC97-H cells after fluphenazine treatment (Fig. 5A), confirming our hypothesis. We also used LysoTracker Red dye to stain HCC cells, observing that fluphenazine markedly reduced the intensity of red fluorescence in the cells, indicating that the acidification function of lysosomes might be inhibited (Fig. 5C).

We also treated the cells with 3-methyladenine (3-MA) and chloroquine (CQ), which are early- and late-stage autophagy inhibitors, respectively, to determine the effect of fluphenazine on autophagy in HCC cells. The results showed that 3-MA, which inhibited autophagosome formation, significantly reversed the inhibitory effect of fluphenazine on the viability of HepG-2 cells (Fig. 5D). Similar results were observed in MHCC97-H cells (Fig. 5E). In contrast, after CQ treatment (a lysosomal alkaline agent), the growth inhibition of HCC cells by fluphenazine was further enhanced (Fig. 5D and E). These results suggest that fluphenazine might inhibit the proliferation of HCC cells by impairing their lysosomal acidification function, resulting in autophagosome accumulation and blocked autophagy flux.

3.5. Target Predicition of Flupehnazine based on SuperPred3

Next, we attempted to preliminarily identify potential targets for fluphenazine in anti-HCC. Using SuperPred3 online tool [26], we found some known strong binders of fluphenazine, including histamine H1 receptor, serotonin 6 receptor and some dopamine receptor (Table 1). Apart from this, we also collected additionally predicted targets of fluphenazine and indications of these targets based on machine learning models (Table 2, Table 3, Supplementary Table 3 and Supplementary Table 4). As can be seen, the probability of fluphenazine binding to some of the targets (such as HERG, Histone deacetylase 8 and DNA-(apurinic or apyrimidinic site) lyase), which are closely related to cancer, is relatively high. These results provide a theoretical basis for discovering the targets for fluphenazine in anti-HCC.

3.6. Fluphenazine suppressed HCC growth in nude mice in vivo

Next, we evaluated the anti-HCC activity of fluphenazine *in vivo* using a subcutaneous xenograft model of MHCC97-H cells in nude mice. On the seventh day after tumor-bearing, we grouped the mice based on tumor volume and intraperitoneally injected fluphenazine once every 2 days (4 or 8 mg/kg; Fig. 6A). The tumor volume growth rate was significantly slower in the fluphenazine treatment groups than in the vehicle group in a dose-dependent manner (Fig. 6B). Consistently, the tumor weights in the 4 and 8 mg/kg fluphenazine-treated groups were 0.85 ± 0.41 g and 0.23 ± 0.09 g, respectively, significantly lower than that of the vehicle group (1.31 ± 0.21 g) (Fig. 6C). In addition, immunohistochemistry (IHC) staining of the tumor tissues showed that fluphenazine significantly inhibited HCC cell proliferation *in vivo*, as reflected by decreased Ki-67 expression levels in the tumor tissues (Fig. 6D and E).

Table 1
Known strong binders of fluphenazine.

Target Name	UniProt ID	Min Activity	Assay type
Dopamine D2 receptor	P14416	1.44 nm	Ki
Dopamine D3 receptor	P35462	3.21 nm	Ki
Dopamine D5 receptor	P21918	21 nm	Ki
Histamine H1 receptor	P35367	40 nm	Ki
Serotonin 6 (5-HT6) receptor	P50406	50 nm	Ki
Dopamine D1 receptor	P21728	179 nm	Ki

Table 2
Top 10 predicted targets of fluphenazine.

Target Name	UniProt ID	Probability	Model accuracy
HERG	Q12809	99.19 %	89.76 %
Nuclear factor NF-kappa-B p105 subunit	P19838	97.99 %	96.09 %
Serotonin 2c (5-HT2c) receptor	P28335	95.71 %	89.62 %
Cathepsin D	P07339	94.96 %	98.95 %
G-protein coupled bile acid receptor 1	Q8TDU6	93.98 %	93.65 %
Endoplasmic reticulum-associated amyloid beta-peptide-binding protein	Q99714	93.05 %	70.16 %
Histone deacetylase 8	Q9BY41	92.87 %	93.99 %
Serotonin transporter	P31645	92.49 %	95.51 %
Tyrosine-protein kinase YES	P07947	92.03 %	83.14 %
Kruppel-like factor 5	Q13887	91.9 %	86.33 %

Table 3
Indications of some predicted targets.

Target Name	Indication	Probability	Model accuracy
HERG	Ovarian cancer	99.19 %	89.76 %
Histone deacetylase 8	Solid tumour/cancer	92.87 %	93.99 %
DNA-(apurinic or apyrimidinic site) lyase	Ocular cancer	87.44 %	91.11 %
DNA-(apurinic or apyrimidinic site) lyase	Solid tumour/cancer	87.44 %	91.11 %
Serotonin 2a (5-HT2a) receptor	Pancreatic cancer	87.38 %	91.43 %
Muscarinic acetylcholine receptor M5	Solid tumour/cancer	85.76 %	94.62 %
Platelet-derived growth factor receptor alpha	Breast cancer	80.93 %	91.07 %
Platelet-derived growth factor receptor alpha	Colon cancer	80.93 %	91.07 %
Platelet-derived growth factor receptor alpha	Colorectal cancer	80.93 %	91.07 %
Platelet-derived growth factor receptor alpha	Gastrointestinal cancer	80.93 %	91.07 %

In addition, we evaluated the safety of fluphenazine *in vivo*. None of the tumor-bearing mice died during the study. The weights of the fluphenazine-treated mice decreased at the beginning of the treatment but recovered to normal (Fig. 7A). On the day after the fifth administration, we tested the motor ability of the mice using the rotating rod method, finding that fluphenazine did not cause motor function loss (Fig. 7B). After 17 days of administration, the liver function indices were tested, and fluphenazine treatment did not affect serum aspartate aminotransferase (AST) or alanine transaminase (ALT) levels (Fig. 7C). Hematoxylin and eosin (H&E) staining also showed that fluphenazine treatment did not damage the important organs (Fig. 7D). Therefore, fluphenazine possesses anti-HCC activity and is safe *in vivo*.

3.7. Fluphenazine alleviated oxaliplatin-induced chronic pain in mice

As a nervous system drug, it is reported that fluphenazine has antiallodynic properties in multiple neuropathic pain [27]. Therefore, we studied the analgesic effect of fluphenazine on the chemotherapeutics-induced chronic pain. We established oxaliplatin-induced chronic pain model in mice and administrated with fluphenazine to observe the pain threshold and behavioral changes (Fig. 8A). At one day after modeling, the data showed that oxaliplatin significantly induced mechanical and thermal allodynia in the ipsilateral hind paws of mice lasting at least 8 days or longer, indicating the accomplishment of modeling (Fig. 8B and C). Administration of fluphenazine significantly alleviated the mechanical and thermal allodynia induced by oxaliplatin reflected as the increased mechanical threshold and thermal latency (Fig. 8B and C).

OF test and EPM test are generally used to evaluate anxiety-like behavior induced by chronic pain in mice. In the OF test, oxaliplatin significantly decreased both time and percentage of moving distance in the central area of mice as compared to control group (Fig. 8D). Consistently, the results showed that oxaliplatin-treated mice obviously traveled shorter time and less entries in the open arm compared with mice in control group as reflected by EPM test (Fig. 8E). However, administration of fluphenazine to oxaliplatin-treated mice reversed these behavioral paradigms, implying fluphenazine not only exert a positive regulation of pain, but also pain-related anxiety-like behavior.

4. Discussion

In recent years, the growth rate of patients with HCC has slowed worldwide. However, owing to the poor prognosis for these patients (the 5-year survival rate is only 18 %), HCC remains the third leading cause of cancer-related deaths worldwide [1]. The rapid development of systemic therapies has prolonged the survival time of patients with HCC to a certain extent, especially the success of TKIs and ICIs. However, not all patients benefit from these systemic therapies. For example, approximately 20 % of patients had to stop taking sorafenib due to intolerable side effects [28], and most patients developed drug resistance within six months [29], considerably limiting the clinical application of sorafenib. Similar phenomena have been observed with ICIs; most patients receiving ICI treatment develop drug resistance, and some are not sensitive to the drugs during the initial treatment (due to primary drug resistance) [30].

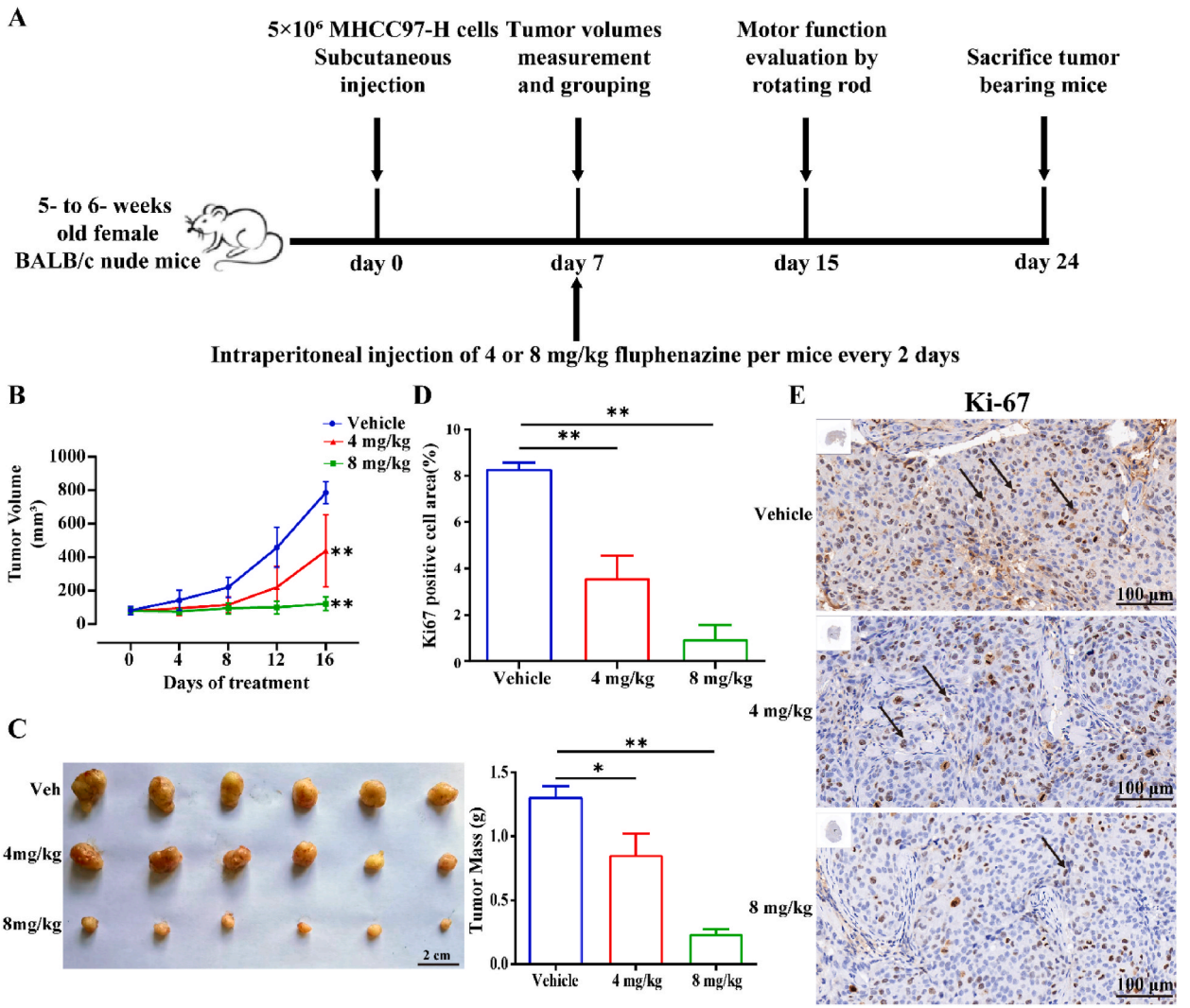

Fig. 6. Fluphenazine inhibited the growth of HCC in mice in the subcutaneous models. (A) The schedule of subcutaneous xenograft model establishment in nude mice. 5×10^6 MHCC97-H cells were injected into left-flanks of 5–6 week old BALB/c nude mice. After injection with cells for 7 days, the mice were grouped based on the tumor volume and administrated with fluphenazine (4 mg/kg or 8 mg/kg) or vehicle once every 2 days i.p. On the other day of the fifth administration, the effect of fluphenazine treatment on motor ability of mice was evaluated using rotating rod method. After 17 days of administration, the mice were sacrificed and the serum, tumor, heart, liver, spleen, lung, kidney and brain were collected. Tumor volumes and body weights of the mice were measured every 4 days. (B) Tumor volume changes in mice during fluphenazine treatment. (C) Tumor size and weight were evaluated after fluphenazine treatment. (D) Quantitative results of the immunohistochemistry (IHC) analysis of Ki-67 expression. (E) The expression of Ki-67 in the tumor tissues was evaluated using IHC analysis. n = 6 mice/group. Data are expressed as mean ± SD (*$P < 0.05$, **$P < 0.01$).

Therefore, novel anti-HCC drug discovery and development are crucial. In this study, we identified fluphenazine as a candidate for HCC based on CMap database. *In vitro* studies showed that fluphenazine suppressed the growth and migration of HCC cells and induced cell cycle arrest and apoptosis. These may be related to its impact on autophagy of HCC cells. Importantly, fluphenazine obviously inhibited the growth of HCC subcutaneous xenografts and did not cause serious side effects *in vivo*. These findings imply that fluphenazine could serve as a new candidate for treating liver cancer.

The therapeutic value of anticancer drugs is based on the magnitude of the clinical benefits. However, only 36.1 % of the drugs approved for the treatment of solid tumors have clinically significant benefits compared to their respective control groups. Furthermore, clinical research for many drugs must be terminated owing to serious side effects [6]. Encouragingly, approved non-oncological drugs have been repurposed for cancer therapy [8]. Almost all drugs have multiple targets; therefore, if these on-the-market drugs possess the same targets as anti-tumor therapies, they will likely have therapeutic effects in patients with cancer. This concept provides excellent opportunities for drug reuse. Establishing TCGA was historic for oncology research as it has provided researchers with many high-throughput genome sequencing results for tumor samples, propelling oncology research and anti-tumor drug development. CMap

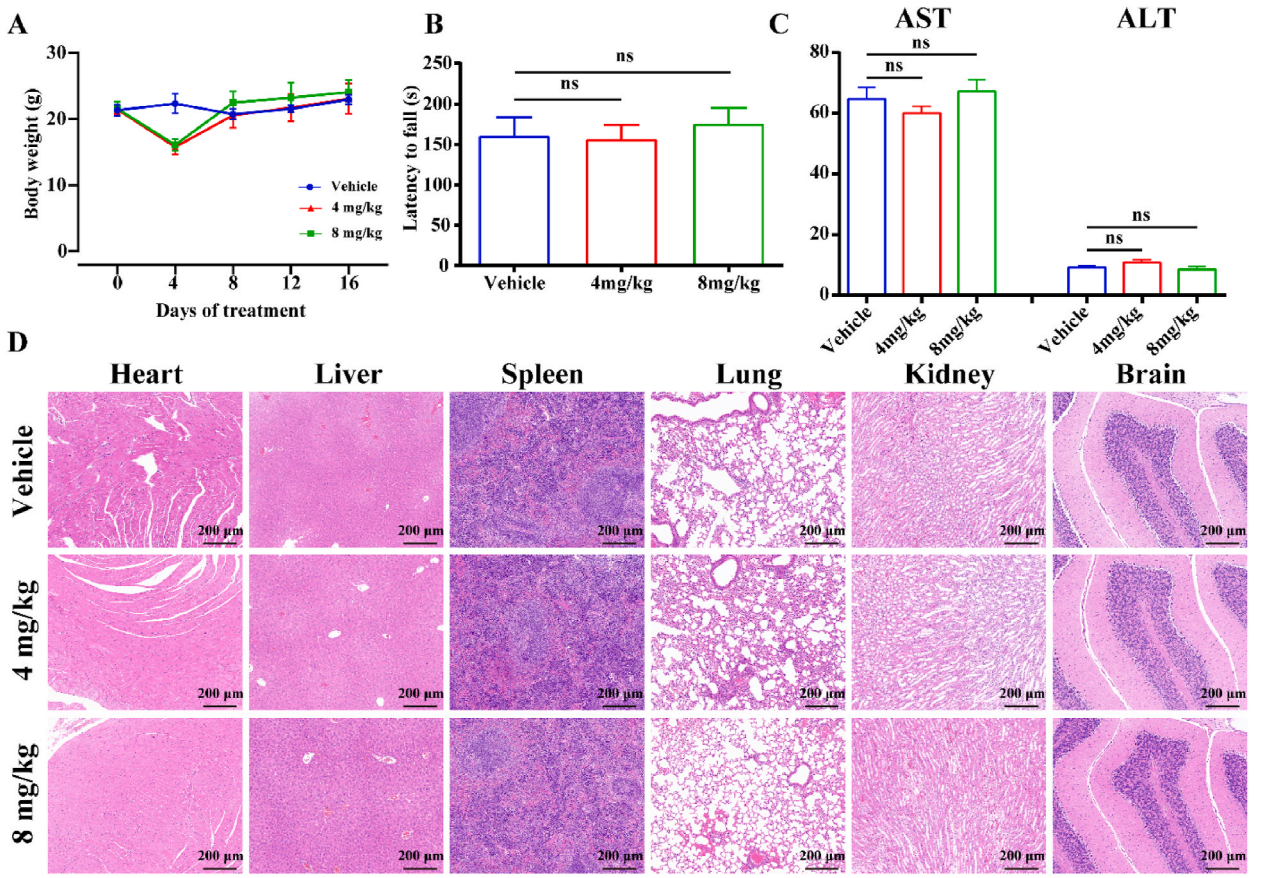

Fig. 7. The safety profiles of fluphenazine in mice with subcutaneous tumor. (A) Body weight changes in mice during fluphenazine treatment. **(B)** On the other day of the fifth administration, the effect of fluphenazine treatment on motor ability of mice was evaluated using rotating rod method. **(C)** After 17 days of administration, the mice were sacrificed and the aspartate aminotransferase and alanine transaminase levels in the blood serum were tested. **(D)** Hematoxylin and eosin stained heart, liver, spleen, lung, kidney and brain of mice after treatment with fluphenazine. n = 6 mice/group. Data are expressed as mean ± SD (ns $P > 0.05$).

is an expression profile database based on the expression of intervention genes developed by the Broad Research Institute [11], providing gene expression profiles of human cell lines before and after drug treatment [12,13]. Therefore, we used TCGA and CMap database data to identify new therapeutic indications for approved or investigational drugs outside their original scope. Briefly, we compared DEGs between tumor and normal tissues obtained from TCGA with the CMap database, obtaining correlation scores from −100 to 100 based on the degree of enrichment; positive scores indicated similarities between the DEGs and genes in the CMap database, whereas negative scores were the opposite. Then, we identified drugs with potential anti-tumor effects by comparing these expression differences.

This study aimed to identify existing drugs with anti-HCC activity that were not originally intended for cancer therapy. By comparing DEGs and using the CMap database, fluphenazine was selected for further investigation after excluding non-approved and HCC-related drugs. Fluphenazine is a classic and widely-used antipsychotic drug. Importantly, recent studies have described fluphenazine as a potential candidate for multiple cancer therapies, such as lung and breast cancer [22,31,32]. However, only a few studies have investigated the anti-HCC activity of fluphenazine. Using high-throughput screening, **Hamid *et al.*** found that fluphenazine inhibited HCC cell viability *in vitro* [33], but in-depth investigations have not been conducted, and the underlying mechanisms remain ambiguous. Consistent with the results of **Hamid *et al.***, our results showed that fluphenazine significantly inhibited growth in the micromolar range and induced G0/G1 phase arrest in HCC cells. An abnormal cell cycle and uncontrolled cell proliferation during mitosis are typical characteristics of cancer [34], and the G1/S cell cycle checkpoint is crucial for determining whether cells enter the S phase of DNA synthesis through the G1 phase [35]. Two cell cycle kinase complexes, CDK4/6-cyclin D and CDK2-cyclin E, work together to inhibit the dynamic transcription complex containing retinoblastoma (Rb) protein and E2F [36]. In the G1 phase of uncommitted cells, low-phosphorylated Rb binds to the E2F-DP1 transcription factor and forms an inhibitory complex with histone deacetylases, inhibiting key downstream transcriptional activity. Entering the S phase is achieved by the continuous phosphorylation of Rb in cyclin D-CDK4/6 and cyclin E-CDK2 [35]. Notably, the cyclin D1/CKD4/6 complex has been studied as a therapeutic target for cancer, and its checkpoint is always unrestricted in human tumors [37]. In the current study, fluphenazine significantly downregulated cyclin D1, cyclin E1, CDK2, and CDK4 expression in HepG-2 and MHCC97-H cells. Additionally, fluphenazine causes P21 and P27

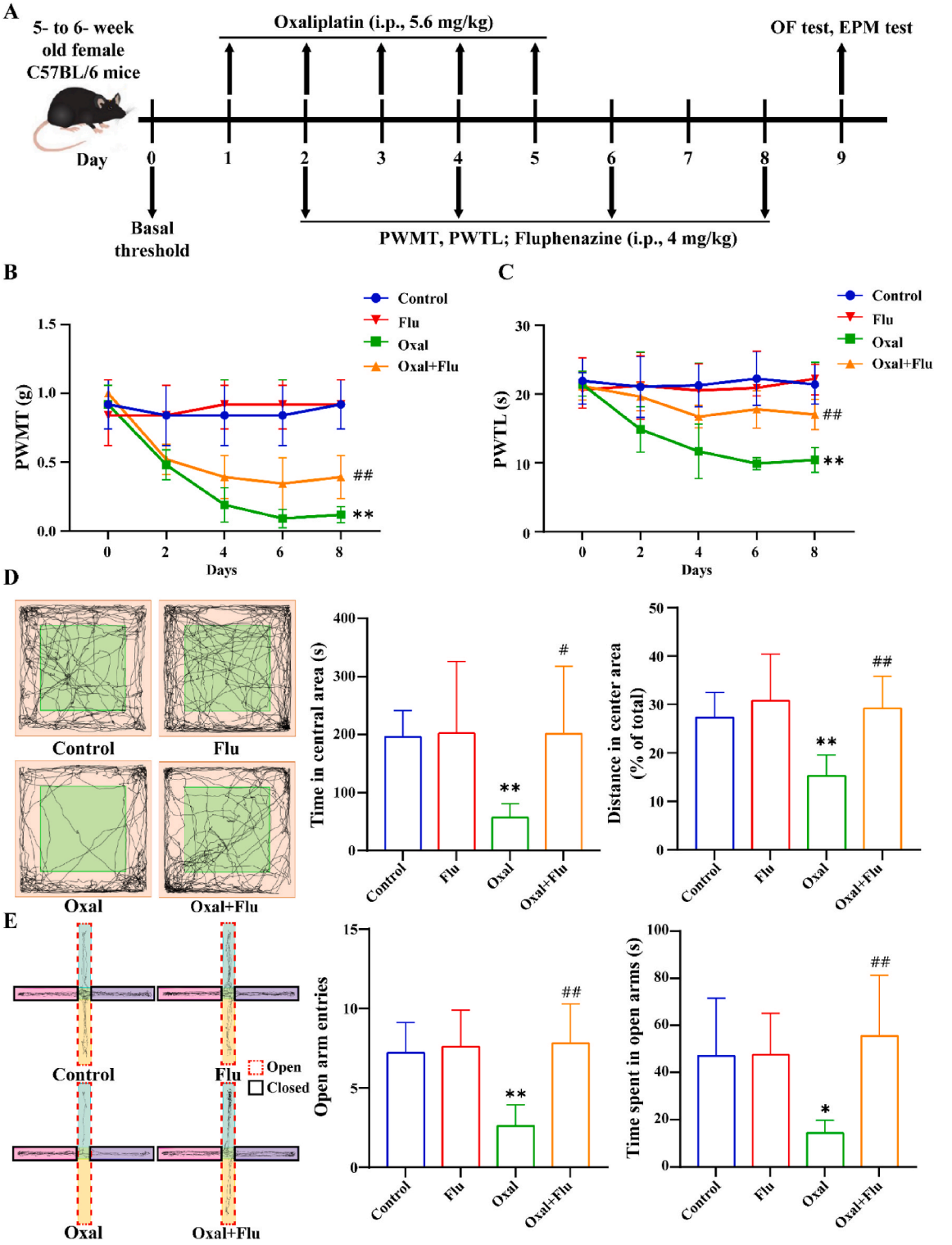

Fig. 8. Fluphenazine ameliorated hypersensitivity of chronic pain and anxiety-like behaviors induced by oxaliplatin in mice. (A) The schedule of experiments. Male C57BL/6 mice were randomly allocated to control or different experimental groups (n = 5). Oxaliplatin or vehicle was injected (i.p.) at 5.6 mg/kg once per day for five consecutive days. From the second day of modeling, fluphenazine or vehicle was injected (i.p.) at 4 mg/kg once every 2 days for four times. PWMT and PWTL were carried out to evaluate hypersensitivity of chronic pain. OF test and EPM test were used to determined anxiety-like behaviors. **(B)** Mechanical pain thresholds of the ipsilateral hind paws following in each group. **(C)** Thermal pain thresholds of the ipsilateral hind paws following oxaliplatin or fluphenazine treatment in each group. **(D)** Schematic traces of the OF test. The

time spent in the central area and percentage of distance moved in the central area (% of total distance traveled) in each group of mice in the OF test. **(E)** Schematic traces of the EPM test. The number of entries into the open arm and the time spent in the open arm in each group of mice in the EPM test. Data are expressed as mean ± SD (*vs* control group $^{*}P < 0.05$, $^{**}P < 0.01$; *vs* oxaliplatin group $^{\#}P < 0.05$, $^{\#\#}P < 0.01$). PWMT, paw withdrawal mechanical threshold; PWTL, paw withdrawal thermal latency; OF test, open field test; EPM test, elevated plus-maze test.

accumulation, two critical inhibitory proteins involved in the G1/S cell cycle transition.

Increased apoptosis is another reason for cell growth inhibition. Cell proliferation requires the suppression of apoptosis by inhibiting the expression of pro-apoptotic factors and inducing the expression of anti-apoptotic factors [38]. In this study, fluphenazine significantly downregulated Bcl-2 and upregulated Bax expression, which have anti- and pro-apoptotic roles, respectively. Furthermore, the downstream effector, caspase-3, was cleaved, which induces apoptosis. We also observed upregulated H2AX phosphorylation (i.e., γ-H2AX), an important DNA damage marker commonly used to evaluate apoptosis. The PI3K pathway also plays an essential role in cell survival by activating Akt. Activated Akt inhibits the activity of pro-apoptotic Bcl-2 family members, such as Bad, Bax, caspase-9, glycogen synthase kinase-3 (i.e., GSK-3), and forkhead box O1 (i.e., FoxO1) [39]. Therefore, fluphenazine's effects on phosphorylated Akt expression were evaluated, showing that fluphenazine significantly decreased the Akt phosphorylation in HCC cells.

Autophagy is a double-edged sword for the occurrence and development of tumors. Under normal conditions, autophagy is thought to prevent cancer. In contrast, once cancer develops, tumor cells provide energy to promote proliferation and inhibit apoptosis by activating autophagy [40]. However, excessive autophagy or blocked autophagy flux can also induce apoptosis [41]. Recent studies have indicated that fluphenazine is a potential autophagy modulator in several cancer cell types [24,25]. Therefore, we speculated that fluphenazine induces apoptosis by regulating autophagy in HCC cells. To test this hypothesis, we detected the expression levels of the autophagic marker, LC3B, finding that it increased after fluphenazine treatment, suggesting that autophagy was activated. However, autophagy is a dynamic process, and the activation and patency of autophagic fluxes are crucial. Changes in the LC3-II levels alone are insufficient to reflect the state of autophagic flux; thus, determining the P62 expression level is also necessary. When autophagic flux is activated, P62 cooperates with the degradation of the product (e.g., [tau]) [42]. In contrast, P62 accumulation leads to upregulation of the product. Our results showed that fluphenazine significantly increased P62 expression, indicating that autophagic flux in HCC cells was blocked. This result was confirmed by the Beclin-1 level, a critical protein for autophagosome formation, which did not change after fluphenazine treatment, suggesting that increased accumulation of LC3 in HCC cells after fluphenazine treatment may be due to blocked autophagy flux rather than autophagy activation. Moreover, using the lysosomal acidity-sensitive dye LysoTracker Red, we found that fluphenazine remarkably reduced the intensity of red fluorescence in cells, indicating that the acidification function of lysosomes may be inhibited. To verify this hypothesis, we administered 3-MA and CQ, which are early and late autophagy inhibitors, respectively. 3-MA and CQ respectively reduced and enhanced the inhibitory effect of fluphenazine on HCC cell proliferation, suggesting that fluphenazine may inhibit cell proliferation by disrupting the lysosomal acidification function of HCC cells, resulting in the autophagosome accumulation and blocked autophagic flux. We also predicted some targets that maybe participate in the anti-HCC effect of fluphenazine using machine learning models, however, the exact anti-HCC target of fluphenazine still needs further study.

In vivo anti-tumor activity is a key indicator when evaluating anti-tumor drugs. Therefore, we also evaluated the anti-HCC activity of fluphenazine *in vivo* using a subcutaneous xenograft model of MHCC97-H cells in nude mice. Due to the significant differences in drug metabolism, absorption, distribution, and excretion processes between actual biological systems *in vivo* and cell models *in vitro*, further drug metabolism and toxicology studies are needed to determine the optimal dosage and regimen before conducting animal experiments *in vivo*. It is generally accepted that the dosage should be one tenth of LD_{50}, and the LD_{50} value of fluphenazine in mice is 89 mg/kg. Combining with previous reports [43], we selected 4 mg/kg or 8 mg/kg (once every two days, i.p.) as dosage regiments. Intraperitoneal fluphenazine injections significantly inhibited tumor growth in nude mice. Furthermore, the safety profile of fluphenazine, an approved drug in clinical use for a long time, was clear; our results confirmed that fluphenazine did not affect motor function, liver function (aminopherase), or other organs after administering 4 mg/kg or 8 mg/kg once every other day. These findings indicate that fluphenazine has good anti-HCC activity and is safe in nude mice.

As is known, some chemotherapeutic drugs (oxaliplatin, paclitaxel et al.) often lead to chronic pain called chemotherapy-induced peripheral neuropathy (CIPNP) [44]. CIPNP occurs acutely during chemotherapy and is frequently accompanied with psychiatric disorders (anxiety and depression et al.). If the patient's symptoms are severe, it may be necessary to reduce the dose of chemotherapy drugs, or even terminate the chemotherapy regimen in advance, which seriously affects the quality of life and survival of tumor patients [45]. Therefore, it would be gratifying to find a drug that not only inhibits tumor growth combination with chemotherapy drugs, but also alleviates the adverse reactions caused by chemotherapy agents. Recent research found that fluphenazine had anti-allodynic properties in multiple neuropathic pain due to the blockage of voltage-gated sodium channels [27]. Therefore, after verifying the anti-HCC activity of fluphenazine, we wonder whether it may exert analgesic effect on chronic pain induced by chemotherapy drugs. We established chronic pain model in mice induced by oxaliplatin, a commonly used chemotherapy agent for advanced HCC patients. Our behavioral analyses revealed that fluphenazine could significantly alleviate oxaliplatin-induced chronic pain and reversed anxiety-like behavioral paradigms in mice, which are findings indicative of its desirable anxiolytic effect in the CNPIP state.

This study had some limitations. For example, the direct anti-HCC target of fluphenazine and the mechanism of fluphenazine in HCC have not been defined, and the anti-HCC effects of fluphenazine in animals with normal immune function require further evaluation.

In conclusion, fluphenazine inhibited HCC cell growth by inducing G0/G1 cell cycle arrest and apoptosis, and its mechanism may be related to the disruption of lysosomal function, leading to the blockage of autophagic flux. Importantly, the most striking finding of

this study was the identification of fluphenazine not only as an anti-HCC drug, but also as an analgesic of chronic pain induced by chemotherapy. Collectively, our findings suggest that fluphenazine is a novel candidate for treating liver cancer.

Grant support

This research was funded by the National Natural Science Foundation of China, China (31800887) and the Key Research and Development Project of Shaanxi Province, China (2023-ZDLSF-59).

Data availability statement

Data included in article/supp. Material/referenced in article.

CRediT authorship contribution statement

Chang Su: Writing – original draft, Visualization, Validation, Methodology, Investigation, Formal analysis, Conceptualization. **Caiyan Cheng:** Visualization, Validation, Methodology, Investigation. **Zheng Rong:** Validation, Software, Investigation. **Jing-cheng Yang:** Formal analysis. **Zhi-mei Li:** Software. **Jing-yue Yao:** Data curation. **An Liu:** Resources. **Le Yang:** Writing – review & editing, Supervision, Project administration, Funding acquisition, Conceptualization. **Ming-gao Zhao:** Writing – review & editing, Supervision, Project administration, Funding acquisition, Conceptualization.

Declaration of competing interest

The authors declare that they have no known competing financial interests or personal relationships that could have appeared to influence the work reported in this paper.

Acknowledgments

We would like to thank Editage (www.editage.cn) for English language editing.

Appendix A. Supplementary data

Supplementary data to this article can be found online at https://doi.org/10.1016/j.heliyon.2023.e22605.

References

[1] World Health Organization, Cancer Today: Cancer Fact Sheets, 2020 [cited 2023 Jan 17]. Available from: https://gco.iarc.fr/today/factsheets-cancers.
[2] G. Sapisochin, L. Castells, C. Dopazo, I. Bilbao, B. Minguez, J.L. Lazaro, et al., Single hcc in cirrhotic patients: liver resection or liver transplantation? Long-term outcome according to an intention-to-treat basis, Ann. Surg Oncol. 20 (4) (2013) 1194–1202, https://doi.org/10.1245/s10434-012-2655-1. Epub 2012/09/12.
[3] J.M. Llovet, S. Ricci, V. Mazzaferro, P. Hilgard, E. Gane, J.F. Blanc, et al., Sorafenib in advanced hepatocellular carcinoma, N. Engl. J. Med. 359 (4) (2008) 378–390, https://doi.org/10.1056/NEJMoa0708857. Epub 2008/07/25.
[4] M. Kudo, R.S. Finn, S. Qin, K.H. Han, K. Ikeda, F. Piscaglia, et al., Lenvatinib versus sorafenib in first-line treatment of patients with unresectable hepatocellular carcinoma: a randomised phase 3 non-inferiority trial, Lancet 391 (10126) (2018) 1163–1173, https://doi.org/10.1016/S0140-6736(18)30207-1. Epub 2018/02/13.
[5] R.S. Finn, S. Qin, M. Ikeda, P.R. Galle, M. Ducreux, T.Y. Kim, et al., Atezolizumab plus bevacizumab in unresectable hepatocellular carcinoma, N. Engl. J. Med. 382 (20) (2020) 1894–1905, https://doi.org/10.1056/NEJMoa1915745. Epub 2020/05/14.
[6] Y. Zhang, A.K. Wagner, X. Guan, Newly approved cancer drugs in China - innovation and clinical benefit, Nat. Rev. Clin. Oncol. (2023), https://doi.org/10.1038/s41571-023-00728-3. Epub 2023/01/17.
[7] S. Pushpakom, F. Iorio, P.A. Eyers, K.J. Escott, S. Hopper, A. Wells, et al., Drug repurposing: progress, challenges and recommendations, Nat. Rev. Drug Discov. 18 (1) (2019) 41–58, https://doi.org/10.1038/nrd.2018.168. Epub 2018/10/13.
[8] Z. Zhang, L. Zhou, N. Xie, E.C. Nice, T. Zhang, Y. Cui, et al., Overcoming cancer therapeutic bottleneck by drug repurposing, Signal Transduct. Targeted Ther. 5 (1) (2020) 113, https://doi.org/10.1038/s41392-020-00213-8. Epub 2020/07/04.
[9] E. Ekinci, S. Rohondia, R. Khan, Q.P. Dou, Repurposing disulfiram as an anti-cancer agent: updated review on literature and patents, Recent Pat. Anti-Cancer Drug Discov. 14 (2) (2019) 113–132, https://doi.org/10.2174/1574892814666190514104035. Epub 2019/05/16.
[10] M. Pollak, Overcoming drug development bottlenecks with repurposing: repurposing biguanides to target energy metabolism for cancer treatment, Nat Med 20 (6) (2014) 591–593, https://doi.org/10.1038/nm.3596. Epub 2014/06/06.
[11] J. Lamb, E.D. Crawford, D. Peck, J.W. Modell, I.C. Blat, M.J. Wrobel, et al., The connectivity map: using gene-expression signatures to connect small molecules, genes, and disease, Science 313 (5795) (2006) 1929–1935, https://doi.org/10.1126/science.1132939. Epub 2006/09/30.
[12] A.M. Brum, J. van de Peppel, C.S. van der Leije, M. Schreuders-Koedam, M. Eijken, B.C. van der Eerden, et al., Connectivity map-based discovery of parbendazole reveals targetable human osteogenic pathway, Proc Natl Acad Sci U S A 112 (41) (2015) 12711–12716, https://doi.org/10.1073/pnas.1501597112. Epub 2015/10/01.
[13] S. Chen, X. Liu, C. Peng, C. Tan, H. Sun, H. Liu, et al., The phytochemical hyperforin triggers thermogenesis in adipose tissue via a dlat-ampk signaling Axis to curb obesity, Cell Metab 33 (3) (2021) 565–580 e7, https://doi.org/10.1016/j.cmet.2021.02.007. Epub 2021/03/04.
[14] Z.L. Luo, S.Q. Cheng, J. Shi, H.L. Zhang, C.Z. Zhang, H.Y. Chen, et al., A splicing variant of merlin promotes metastasis in hepatocellular carcinoma, Nat. Commun. 6 (2015) 8457, https://doi.org/10.1038/ncomms9457. Epub 2015/10/08.
[15] B. Yang, M. Li, W. Tang, W. Liu, S. Zhang, L. Chen, et al., Dynamic network biomarker indicates pulmonary metastasis at the tipping point of hepatocellular carcinoma, Nat. Commun. 9 (1) (2018) 678, https://doi.org/10.1038/s41467-018-03024-2. Epub 2018/02/16.

[16] A. Francois, S.A. Low, E.I. Sypek, A.J. Christensen, C. Sotoudeh, K.T. Beier, et al., A brainstem-spinal cord inhibitory circuit for mechanical pain modulation by gaba and enkephalins, Neuron 93 (4) (2017) 822–839, https://doi.org/10.1016/j.neuron.2017.01.008, e6. Epub 2017/02/07.

[17] Y.Y. Chen, K.S. Jiang, X.H. Bai, M. Liu, S.Y. Lin, T. Xu, et al., Zeb1 induces Ddr1 promoter hypermethylation and contributes to the chronic pain in spinal cord in rats following oxaliplatin treatment, Neurochem. Res. 46 (8) (2021) 2181–2191, https://doi.org/10.1007/s11064-021-03355-5. Epub 2021/05/26.

[18] C.A. Fairbanks, Spinal delivery of analgesics in experimental models of pain and analgesia, Adv. Drug Deliv. Rev. 55 (8) (2003) 1007–1041, https://doi.org/10.1016/s0169-409x(03)00101-7. Epub 2003/08/26.

[19] A.F. Bourquin, M. Süveges, M. Pertin, N. Gilliard, S. Sardy, A.C. Davison, et al., Assessment and analysis of mechanical allodynia-like behavior induced by spared nerve injury (sni) in the mouse, Pain 122 (1–2) (2006), https://doi.org/10.1016/j.pain.2005.10.036, 14.e1-. Epub 2006/03/18.

[20] K. Hargreaves, R. Dubner, F. Brown, C. Flores, J. Joris, A new and sensitive method for measuring thermal nociception in cutaneous hyperalgesia, Pain 32 (1) (1988) 77–88, https://doi.org/10.1016/0304-3959(88)90026-7. Epub 1988/01/01.

[21] A.K. Kraeuter, P.C. Guest, Z. Sarnyai, The open field test for measuring locomotor activity and anxiety-like behavior, Methods Mol. Biol. 1916 (2019) 99–103, https://doi.org/10.1007/978-1-4939-8994-2_9. Epub 2018/12/12.

[22] M.A. Goyette, R. Cusseddu, I. Elkholi, A. Abu-Thuraia, N. El-Hachem, B. Haibe-Kains, et al., Axl knockdown gene signature reveals a drug repurposing opportunity for a class of antipsychotics to reduce growth and metastasis of triple-negative breast cancer, Oncotarget 10 (21) (2019) 2055–2067, https://doi.org/10.18632/oncotarget.26725. Epub 2019/04/23.

[23] M.H. Cardone, N. Roy, H.R. Stennicke, G.S. Salvesen, T.F. Franke, E. Stanbridge, et al., Regulation of cell death protease caspase-9 by phosphorylation, Science 282 (5392) (1998) 1318–1321, https://doi.org/10.1126/science.282.5392.1318. Epub 1998/11/13.

[24] Y. Li, S. McGreal, J. Zhao, R. Huang, Y. Zhou, H. Zhong, et al., A cell-based quantitative high-throughput image screening identified novel autophagy modulators, Pharmacol. Res. 110 (2016) 35–49, https://doi.org/10.1016/j.phrs.2016.05.004. Epub 2016/05/12.

[25] D. Zong, K. Zielinska-Chomej, T. Juntti, B. Mork, R. Lewensohn, P. Haag, et al., Harnessing the lysosome-dependent antitumor activity of phenothiazines in human small cell lung cancer, Cell Death Dis. 5 (3) (2014) e1111, https://doi.org/10.1038/cddis.2014.56. Epub 2014/03/15.

[26] J. Nickel, B.O. Gohlke, J. Erehman, P. Banerjee, W.W. Rong, A. Goede, et al., Superpred: update on drug classification and target prediction, Web Server issue), Nucleic Acids Res. 42 (2014) W26–W31, https://doi.org/10.1093/nar/gku477. Epub 2014/06/01.

[27] X.W. Dong, Y. Jia, S.X. Lu, X. Zhou, M. Cohen-Williams, R. Hodgson, et al., The antipsychotic drug, fluphenazine, effectively reverses mechanical allodynia in rat models of neuropathic pain, Psychopharmacology (Berl) 195 (4) (2008) 559–568, https://doi.org/10.1007/s00213-007-0942-5. Epub 2007/09/25.

[28] J.A. Marrero, M. Kudo, A.P. Venook, S.L. Ye, J.P. Bronowicki, X.P. Chen, et al., Observational registry of sorafenib use in clinical practice across child-pugh subgroups: the gideon study, J. Hepatol. 65 (6) (2016) 1140–1147, https://doi.org/10.1016/j.jhep.2016.07.020. Epub 2016/07/30.

[29] W. Tang, Z. Chen, W. Zhang, Y. Cheng, B. Zhang, F. Wu, et al., The mechanisms of sorafenib resistance in hepatocellular carcinoma: theoretical basis and therapeutic aspects, Signal Transduct. Targeted Ther. 5 (1) (2020) 87, https://doi.org/10.1038/s41392-020-0187-x. Epub 2020/06/14.

[30] G. Morad, B.A. Helmink, P. Sharma, J.A. Wargo, Hallmarks of response, resistance, and toxicity to immune checkpoint blockade, Cell 184 (21) (2021) 5309–5337, https://doi.org/10.1016/j.cell.2021.09.020. Epub 2021/10/09.

[31] D. Zong, P. Haag, I. Yakymovych, R. Lewensohn, K. Viktorsson, Chemosensitization by phenothiazines in human lung cancer cells: impaired resolution of Gammah2ax and increased oxidative stress elicit apoptosis associated with lysosomal expansion and intense vacuolation, Cell Death Dis. 2 (7) (2011) e181, https://doi.org/10.1038/cddis.2011.62. Epub 2011/07/22.

[32] K. Sroda-Pomianek, K. Michalak, A. Palko-Labuz, A. Uryga, P. Swiatek, M. Majkowski, et al., The combined use of phenothiazines and statins strongly affects doxorubicin-resistance, apoptosis, and cox-2 activity in colon cancer cells, Int. J. Mol. Sci. 20 (4) (2019), https://doi.org/10.3390/ijms20040955. Epub 2019/03/01.

[33] R. Hamid, Y. Rotshteyn, L. Rabadi, R. Parikh, P. Bullock, Comparison of alamar blue and mtt assays for high through-put screening, Toxicol. Vitro 18 (5) (2004) 703–710, https://doi.org/10.1016/j.tiv.2004.03.012. Epub 2004/07/15.

[34] D. Hanahan, R.A. Weinberg, Hallmarks of cancer: the next generation, Cell 144 (5) (2011) 646–674, https://doi.org/10.1016/j.cell.2011.02.013. Epub 2011/03/08.

[35] M. Malumbres, M. Barbacid, Cell cycle, cdks and cancer: a changing paradigm, Nat. Rev. Cancer 9 (3) (2009) 153–166, https://doi.org/10.1038/nrc2602. Epub 2009/02/25.

[36] S. van den Heuvel, N.J. Dyson, Conserved functions of the prb and E2f families, Nat. Rev. Mol. Cell Biol. 9 (9) (2008) 713–724, https://doi.org/10.1038/nrm2469. Epub 2008/08/23.

[37] A. Besson, S.F. Dowdy, J.M. Roberts, Cdk inhibitors: cell cycle regulators and beyond, Dev. Cell 14 (2) (2008) 159–169, https://doi.org/10.1016/j.devcel.2008.01.013. Epub 2008/02/13.

[38] G. Brumatti, M. Salmanidis, P.G. Ekert, Crossing paths: interactions between the cell death machinery and growth factor survival signals, Cell. Mol. Life Sci. 67 (10) (2010) 1619–1630, https://doi.org/10.1007/s00018-010-0288-8. Epub 2010/02/17.

[39] Y. Rong, C.W. Distelhorst, Bcl-2 protein family members: versatile regulators of calcium signaling in cell survival and apoptosis, Annu. Rev. Physiol. 70 (2008) 73–91, https://doi.org/10.1146/annurev.physiol.70.021507.105852. Epub 2007/08/08.

[40] J.M.M. Levy, C.G. Towers, A. Thorburn, Targeting autophagy in cancer, Nat. Rev. Cancer 17 (9) (2017) 528–542, https://doi.org/10.1038/nrc.2017.53. Epub 2017/07/29.

[41] R. Amaravadi, A.C. Kimmelman, E. White, Recent insights into the function of autophagy in cancer, Genes Dev. 30 (17) (2016) 1913–1930, https://doi.org/10.1101/gad.287524.116. Epub 2016/09/25.

[42] M. Ono, M. Komatsu, B. Ji, Y. Takado, M. Shimojo, T. Minamihisamatsu, et al., Central role for P62/sqstm1 in the elimination of toxic tau species in a mouse model of tauopathy, Aging Cell 21 (7) (2022), e13615, https://doi.org/10.1111/acel.13615. Epub 2022/06/07.

[43] F. Xu, Y. Xia, Z. Feng, W. Lin, Q. Xue, J. Jiang, et al., Repositioning antipsychotic fluphenazine hydrochloride for treating triple negative breast cancer with brain metastases and lung metastases, Am. J. Cancer Res. 9 (3) (2019) 459–478. Epub 2019/04/06.

[44] N. Majithia, C.L. Loprinzi, T.J. Smith, New practical approaches to chemotherapy-induced neuropathic pain: prevention, assessment, and treatment, Oncology (Williston Park) 30 (11) (2016) 1020–1029. Epub 2016/11/18.

[45] S.J.L. Flatters, P.M. Dougherty, L.A. Colvin, Clinical and preclinical perspectives on chemotherapy-induced peripheral neuropathy (cipn): a narrative review, Br. J. Anaesth. 119 (4) (2017) 737–749, https://doi.org/10.1093/bja/aex229. Epub 2017/11/10.